Applied Physics Letters

Direct observation of ferroelectricity in $Ca_3Mn_2O_7$ and its prominent light absorption

Cite as: Appl. Phys. Lett. **113**, 022902 (2018); https://doi.org/10.1063/1.5037525
Submitted: 25 April 2018 • Accepted: 15 June 2018 • Published Online: 10 July 2018

Meifeng Liu, Yang Zhang, Ling-Fang Lin, et al.

Direct observation of ferroelectricity in $Ca_3Mn_2O_7$ and its prominent light absorption

Meifeng Liu,[1,2] Yang Zhang,[3] Ling-Fang Lin,[3] Lin Lin,[2] Shengwei Yang,[4] Xiang Li,[1,2] Yu Wang,[1] Shaozhen Li,[5] Zhibo Yan,[2] Xiuzhang Wang,[1] Xiao-Guang Li,[4] Shuai Dong,[3,a)] and Jun-Ming Liu[1,2,6]

[1]*Institute for Advanced Materials, Hubei Normal University, Huangshi 435002, China*
[2]*Laboratory of Solid State Microstructures and Innovative Center of Advanced Microstructures, Nanjing University, Nanjing 210093, China*
[3]*School of Physics, Southeast University, Nanjing 211189, China*
[4]*Hefei National Laboratory for Physical Sciences at the Microscale, Department of Physics, University of Science and Technology of China, Hefei 230026, China*
[5]*School of Physics and Institute for Quantum Materials, Hubei Polytechnic University, Huangshi 435003, China*
[6]*Institute for Advanced Materials and Laboratory of Quantum Engineering and Materials, South China Normal University, Guangzhou 510006, China*

(Received 25 April 2018; accepted 15 June 2018; published online 10 July 2018)

Layered perovskites $A_3M_2O_7$ are known to exhibit the so-called hybrid improper ferroelectricity. Despite experimentally confirmed cases (e.g., nonmagnetic M = Ti and Sn), the ferroelectricity in magnetic $Ca_3Mn_2O_7$ remains a puzzle. Here, the structural, ferroelectric, magnetoelectric, and optical properties of $Ca_3Mn_2O_7$ are systematically investigated. Switchable polarization is directly measured, demonstrating its ferroelectricity. In addition, magnetoelectric response is also evidenced, implying the coupling between magnetism and ferroelectricity. Furthermore, strong visible light absorption is observed, which can be understood from its electronic structure. Its direct and appropriate bandgap, as well as wide conducting bands, makes $Ca_3Mn_2O_7$ a potential candidate for ferroelectric photoelectric applications. *Published by AIP Publishing.*
https://doi.org/10.1063/1.5037525

The so-called 327-type Ruddlesden-Popper perovskites with generic chemical formula $A_3M_2O_7$ (A: rare earth or alkaline earth and M: transition metal) have been attracting great research attention since the prediction of hybrid improper ferroelectricity in 2011.[1] In these hybrid improper ferroelectrics, the ferroelectric polar mode couples with and is driven by other nonpolar modes of structural distortions.[1–7] Such hybrid improper ferroelectricity not only expands the scope of ferroelectric materials but also provides potential functions like electric-control of magnetization.

In this category, the first predicted two materials are $Ca_3Ti_2O_7$ and $Ca_3Mn_2O_7$.[1] Structurally, these two materials are very similar, as shown in Fig. S1 of the supplementary material. The condensation of oxygen octahedral rotation and tilting modes leads to the $A2_1am$ space group as the ground state, whose polarization (P) points along the a-axis. The predicted Ps were $\sim 20\,\mu C/cm^2$ for $Ca_3Ti_2O_7$ and $\sim 5\,\mu C/cm^2$ for $Ca_3Mn_2O_7$.[1] The intrinsic magnetoelectric coupling was also expected in $Ca_3Mn_2O_7$.[1]

Soon after the theoretical prediction, the experiment performed by Oh *et al.* confirmed the ferroelectricity in $Ca_3Ti_2O_7$, although the experimentally measured $P \sim 10\,\mu C/cm^2$ is somewhat lower than the expected value.[8] Similar ferroelectricity was also predicted and later observed in $Sr_3Sn_2O_7$.[5,9] However, the direct experimental measurement of ferroelectricity remains absent for $Ca_3Mn_2O_7$. In fact, an experimental study on Mn substituted $Ca_3Ti_2O_7$, i.e., $Ca_3Ti_{2-x}Mn_xO_7$, found suppressed ferroelectricity, i.e., reduced P and lowered transition temperature (T_C), upon increasing the concentration of Mn.[10] The temperature (T)-dependent structural evolution of $Ca_3Mn_2O_7$ is more complex than that of $Ca_3Ti_2O_7$. For example, a phase coexistence over large T range and the "symmetry trapping" of a soft mode were observed.[11,12]

In this work, the high quality polycrystalline samples of $Ca_3Mn_2O_7$ were prepared by the standard solid state reaction method, starting from the highly purified powders of $CaCO_3$ and MnO_2. The stoichiometric mixtures were ground and fired at 1200 °C for 24 h in air. Then, the resultant powders were pelletized into a disk of 2 cm in diameter under 5000 psi pressure and sintered at 1350 °C for 24 h with the intermittent grinding step.

The crystal structure was characterized by X-ray diffraction (XRD) with Cu-K_α radiation from 207 K to 673 K. Using the GSAS Rietveld program,[13] the refined crystallographic information of $Ca_3Mn_2O_7$ is summarized in Table I. At high Ts (e.g., 673 K), the structure can be described by the $I4/mmm$ space group. In contrast, the $A2_1am$ space group can well describe the low T (e.g., 207 K) structure. Such a structural transition from nonpolar $I4/mmm$ to polar $A2_1am$

TABLE I. Lattice constants (in unit of Å) of $Ca_3Mn_2O_7$ determined by Rietveld analysis at low and high Ts (in unit of K).

T	Group	a	b	c	R_{WP} (%)	R_P (%)	χ^2
207	$A2_1am$	5.2423	5.2402	19.3542	8.32	6.42	1.755
673	$I4/mmm$	3.7096	3.7096	19.5050	8.98	6.95	1.969

a)Electronic mail: sdong@seu.edu.cn

agrees with previous reports.[11,12] In the middle T range (e.g., ~300–600 K), the mixture of multiple structures including $I4/mmm$, $A2_1am$, and the intermediate $Amam$ is evidenced, further confirming the complicated structural evolution from paraelectric to ferroelectric states.

In the following, the low T polar $A2_1am$ structure is studied to verify its multiferroicity. The XRD pattern at 207 K is shown in Fig. 1(a). The refined lattice constants (using the $A2_1am$ space group) as a function of T below 300 K are shown in Fig. 1(b). For lattice constants a and b, simultaneous sudden drops are evidenced around 240 K.

To measure the dielectric and ferroelectric properties, the sample was polished into a thin plate with a typical thickness of 0.20 mm and an area of ~7.06 mm^2. The gold electrodes were deposited on the top/bottom surfaces. The dielectric constant ε at different frequencies is measured as a function of T using an HP4294A impedance analyzer, as shown in Fig. 1(c). The variable-T environment is provided by a Physical Property Measurement System (PPMS) of Quantum Design, which can cover 1.8–300 K. A broad peak of ε is observed at ~240 K, coinciding with the sudden drops of in-plane lattice constants [Fig. 1(b)]. The peak slightly shifts to the high T direction with increasing frequency. These characteristics seem to suggest relaxor behavior, which is reasonable considering the large T range of phase coexistence.[11,12] The dielectric loss is very small at low T but becomes considerable large when $T > 100$ K due to serious leakage. This may be the reason why previous experiments were failed to directly measure the ferroelectric P at high T. Such a large dielectric loss at ~240 K also brings somewhat uncertainness regarding T_C, which needs further experimental verifications.

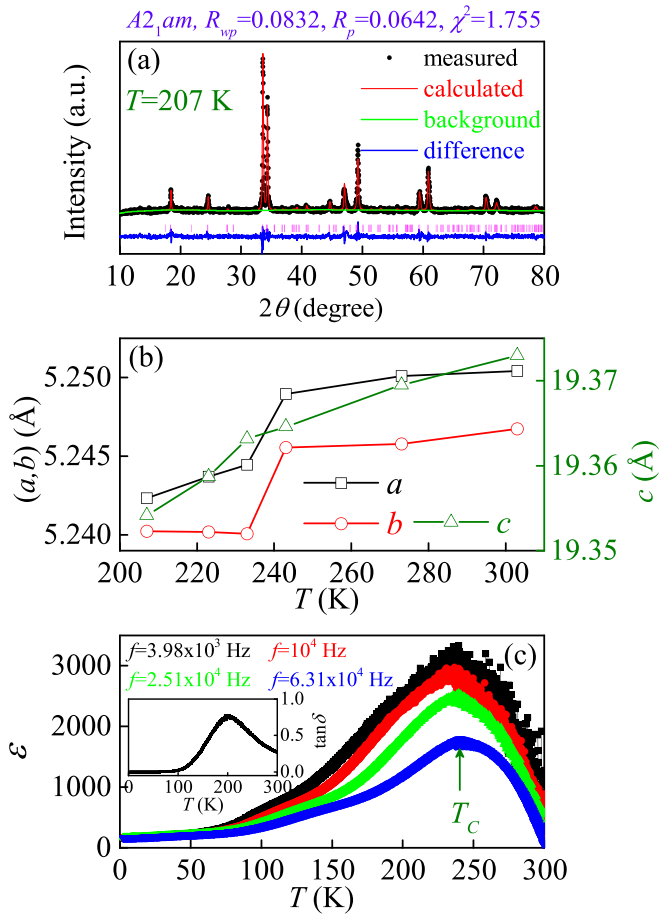

FIG. 1. (a) Rietveld fitting of the low-T powder XRD spectrum for $Ca_3Mn_2O_7$. (b) T-dependent evolution of lattice constants. (c) T-dependent dielectric constant. f: measuring frequency. Inset: the dielectric loss.

The T-dependent ferroelectric P was measured using the pyroelectric current method. In detail, the sample was first poled under a poling electric field from 300 K to 2 K. Then, the electric field was set to zero, and the sample was electrically short-circuited for several hours at 2 K in order to exclude possible extrinsic contributions (e.g., trapped charge during the poling process). Then, the pyroelectric current (I_{pyro}) was collected by heating the sample at different rates of 2, 4, and 6 K/min, as shown in Fig. 2(a). All peaks of I_{pyro}-T curves are exactly at the same position without any shift. Since the current signal increases rapidly when T is above 60 K which may be contributed by the extrinsic thermal excitation, the reliable pyroelectric signal in our work is limited to the low T (<60 K) region. Note that it does not mean that the ferroelectric T_C is 60 K.

Under the poling field of 10 kV/cm, the integrated pyroelectric ΔP is about 2500 $\mu C/m^2$ from 60 K to 2 K for the polycrystalline sample. The integrated pyroelectric ΔP is also independent of the warming rates. The pyroelectric

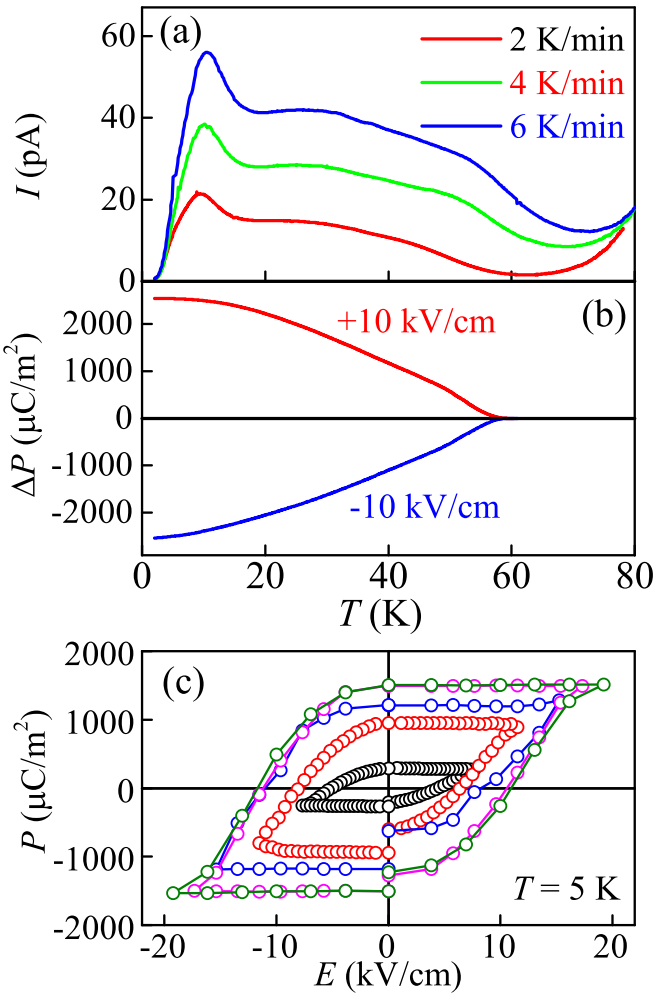

FIG. 2. (a) Raw data of pyroelectric current I_{pyro} as a function of T at three warming rates 2, 4, and 6 K/min, respectively. (b) Integrated pyroelectric ΔP (from 2 K to 60 K) under positive and negative poling electric fields (±10 kV/cm). (c) The ferroelectric hysteresis loops measured at 5 K by the PUND method with different peak voltages.

curves are also measured under the positive and negative poling electric fields. The antisymmetrical pyroelectric curves upon the positive/negative poling fields indicate the reversibility of ΔP, as shown in Fig. 2(b). All these characteristics imply that the measured signals indeed come from the intrinsic ferroelectricity, although some extrinsic factors may also co-exist and contribute to a portion of ΔP. It should be noted that such ΔP is only a part of total P since the ferroelectric T_C is much higher than 60 K.

In addition to the pyroelectric measurement, the ferroelectric hysteresis loops have also been measured using the improved Positive-Up-Negative-Down (PUND) method, which can deduct the extrinsic contribution from leakage and capacitance to some extent. The PUND loop at 5 K is shown in Fig. 2(c), which unambiguously demonstrates the ferroelectricity of $Ca_3Mn_2O_7$. With increasing T, the PUND loops gradually shrink and becomes unmeasurable due to serious leakage when $T > 28$ K (Fig. S2 of the supplementary material).

The magnetic susceptibilities (χs) as a function of T under the zero-field cooling (ZFC) and field-cooling (FC) modes were measured under a small magnetic field of 500 Oe using a superconducting quantum interference device (SQUID) magnetometer (Quantum Design, Inc.), as shown in Fig. 3(a). The peaks of χs appear at 112 K, and the ZFC and FC curves diverge at this point, indicating an antiferromagnetic transition T_N, in agreement with the previous literature.[11,14] The specific heat measurement also exhibits a weak anomaly at this T_N (Fig. S3 of the supplementary material). According to the Curie-Weiss fitting above T_N, the effective magnetic moment is 3.17 μ_B/Mn, close to the expected value of spin-only magnetic moment (3 μ_B/Mn) for the high-spin Mn^{4+} $\left(S_z = \frac{3}{2}\right)$.

Figure 3(b) shows the magnetic hysteresis loops measured at different Ts. Below T_N, weak FM (wFM) type loops are observed, while a paramagnetic loop is evidenced above T_N. According to the theoretical prediction, a net magnetization of $M \sim 0.045$ μ_B/Mn can be generated due to the spin canting of antiferromagnetic background.[1] Here, the residual M is about 0.0025 μ_B/Mn at 10 K. The value of M increases continuously with the magnetic field, which is not saturated even under a high field up to 6.5 T (Fig. S3 of the supplementary material).

In the original theoretical work, the spin-lattice mediated magnetoelectric coupling was predicted, which might lead to electric-control of M.[1] Here, we have investigated the magnetic properties of $Ca_3Mn_2O_7$ under the electric field in the DC excitation mode in SQUID. After the FC (with 4 T magnetic field and 10 kV/cm electric field) from 150 K to 10 K, M (under 4 T) is monitored upon the application of the electric field. As shown in Fig. 3(c), M decreases suddenly when the electric field reaches up to a critical value $E_C \sim 6.25$ kV/cm. Below this critical value, M is quite robust. Although the Joule heat effect may also suppress M, it cannot explain the sudden change and critical field. Interestingly, the ferroelectric coercive field at 10 K is ~6 kV/cm (Fig. S2 of the supplementary material), very close to this E_C, implying that the switching of ferroelectric domains may affect the alignment of magnetic moments. If so, Fig. 3(c) can reflect the magnetoelectricity. Further deeper investigation of magnetoelectricity needs the single crystalline samples since the magnetoelectric response is orientation-dependent. Upon a 10 kV/cm electric field, M decreases for ~3%.

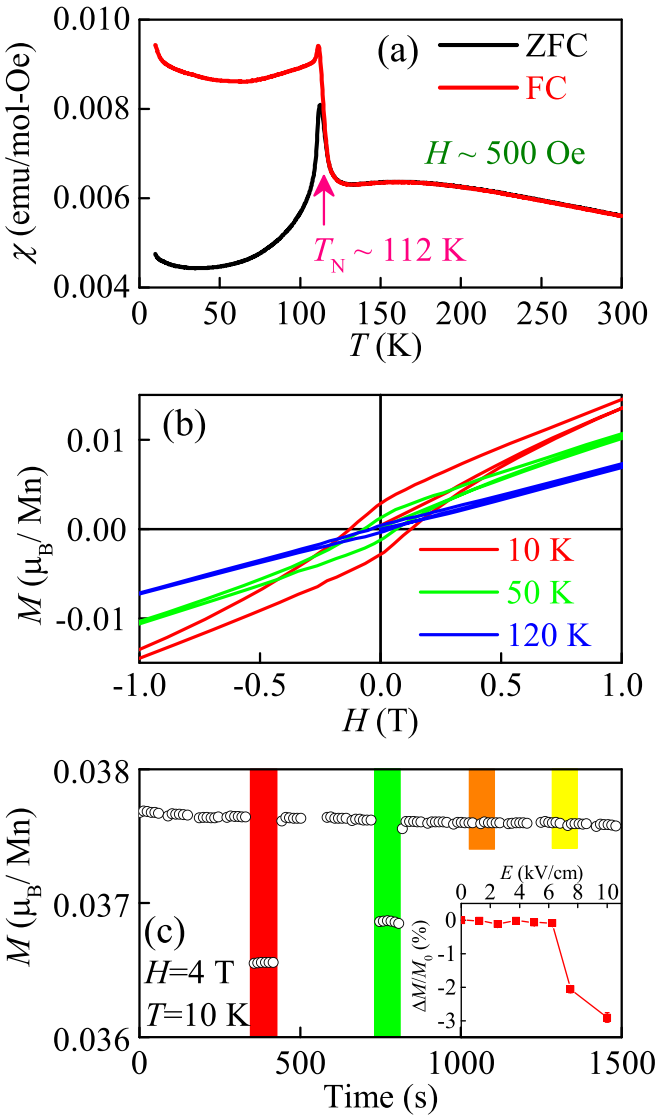

FIG. 3. (a) The magnetic susceptibilities indicate an antiferromagnetic transition at 112 K. (b) The magnetic hysteresis loops at different Ts. (c) Evolution of M under 4 T field at 10 K as a function of time. The color regions denote the periods with electric fields E (red: 10 kV/cm; green: 7.5 kV/cm; orange: 5.0 kV/cm; yellow: 2.5 kV/cm). Inset: Evolution of M as a function of E. The critical field is ~6.25 kV/cm, only beyond which M can be affected.

Recently, photovoltaic effects in ferroelectric (or polar) materials have attracted considerable attention.[16–19] The most attractive advantage of ferroelectric materials is that the internal electric field built by spontaneous P can promote the separation of photo-generated electrons/holes.[20] However, for most ferroelectric materials, there are also some disadvantages, including (1) too large bandgaps or indirect bandgaps, which prevent the efficient absorption of visible light; (2) low mobility of carriers and too large resistivity, which suppress the photo-generated current. These drawbacks obstruct the applications of ferroelectric materials in the photo-electric field.

However, as stated before, $Ca_3Mn_2O_7$ is not very insulating, which is a disadvantage for the ferroelectric measurement but may be an advantage for photovoltaic current or

other photo applications. To characterize the optical properties of $Ca_3Mn_2O_7$, the UV-Vis-NIR diffuse reflectance spectrum was measured at room T with a Cary 5000 UV-Vis-NIR spectrophotometer in the 200–2500 nm wavelength range. The reflectance spectrum was further converted to absorbance with the Kubelka-Munk function.[21] As shown in Fig. 4(a), the Kubelka-Munk function $F(R)$ shows the absorption edge ~1.29 eV (in the infrared light region). The optical bandgap for $Ca_3Mn_2O_7$ has not been reported before. The sample is black with very excellent absorbance of visible light.

To further understand the optical properties, a calculation based on density function theory (DFT) is performed. Although an early DFT calculation had been done for $Ca_3Mn_2O_7$, they used the pure generalized gradient approximation (GGA) without U, which led to an unrealistic too small bandgap (~0.3 eV).[22] Here, our DFT calculations are performed using the projector augmented wave (PAW) pseudopotentials as implemented in the Vienna *ab initio* Simulation Package (VASP) code.[23–26] To acquire more accurate description of crystalline structure and electron correlation, the revised Perdew-Burke-Ernzerhof for solids (PBEsol) function and the GGA + U method are adopted.[26,27] According to the literature,[1] the on-site Coulomb $U_{eff} = 4$ eV is applied to the 3d orbital of Mn, using the Dudarev implementation.[28] The cutoff of the plane wave basis is fixed to 550 eV. The Monkhorst-Pack k-point mesh is $7 \times 7 \times 2$.

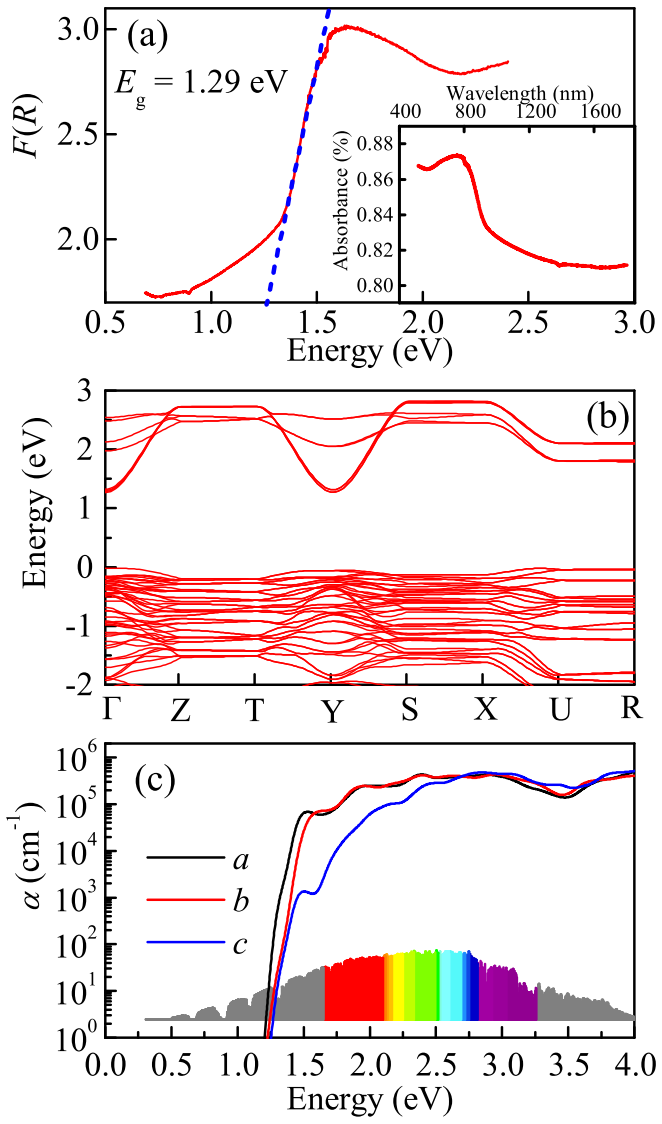

FIG. 4. (a) The Kubelka-Munk functions $F(R)$ as a function of photon energy. The derived optical bandgap is 1.29 eV. Inset: the absorbance of $Ca_3Mn_2O_7$. (b) The GGA + U calculated band structure for the ground magnetic state. (c) The calculated light absorption spectra. Different colors are for the electric field components of light along different axes. The standard AM1.5G solar spectrum is shown at the bottom as a reference.[15]

The DFT band structure shown in Fig. 4(b) demonstrates semiconducting properties with direct bandgaps (~1.3 eV, close to the experimental value) at the Γ and Y points. In addition to the appropriate value of bandgaps, the conducting bands formed by the e_g orbitals are relatively wider (compared with h-$TbMnO_3$[19] and CaOFeS[17]), implying a relatively large mobility of electrons in the ab plane.

Then, the light absorption spectra are calculated from the imaginary part of the dielectric constant,[17,19] as shown in Fig. 4(c). The absorption is better for lights with in-plane electric field components. It is quite nature to understand the anisotropic absorption due to the crystal anisotropy. The in-plane hybrid improper ferroelectricity also leads to tiny anisotropy between the a and b axes for the in-plane electric field components. The first peak of absorption appears near 1.3 eV. Strong absorption in the whole visible light range is found in our calculation. All these characteristics agree with aforementioned experimental results. Further photoelectric measurements on $Ca_3Mn_2O_7$ are encouraged to check its potential applications as a ferroelectric photovoltaic material.

In summary, the physical properties of $Ca_3Mn_2O_7$ have been investigated, including its structural property, magnetism, ferroelectricity, magnetoelectricity, and optical property. Measurements of dielectric constants and the structure suggest possible ferroelectric T_C around 240 K, although the relaxor like behaviors are found in a quite wide temperature range. The ferroelectric polarization is measured at low temperature by the pyroelectric method as well as the PUND method, the latter of which can give the hysteresis loops of electric-polarization. Furthermore, the net magnetization of weak ferromagnetism is evidenced, which can be modulated by the electric field beyond the ferroelectric coercive field. Finally, the strong light absorption has been confirmed in both experiment and DFT calculation, implying potential ferroelectric photo-electric applications.

See supplementary material for the structures and more experimental data of $Ca_3Mn_2O_7$.

This work was supported by the National Key Research Projects of China (Grant No. 2016YFA0300101), the National Natural Science Foundation of China (Grant Nos. 11704109, 11674055, 51431006, 51332006, 51721001, 11504048, and 51790491), and the Research Project of Hubei Provincial Department of Education (Grant No. Q20172501). Most calculations were supported by National Supercomputer Center in Guangzhou (Tianhe II).

[1]N. A. Benedek and C. J. Fennie, Phys. Rev. Lett. **106**, 107204 (2011).
[2]E. Bousquet, M. Dawber, N. Stucki, C. Lichtensteiger, P. Hermet, S. Gariglio, J.-M. Triscone, and P. Ghosez, Nature (London) **452**, 732 (2008).

[3]J. M. Rondinelli and C. J. Fennie, Adv. Mater. **24**, 1961 (2012).
[4]N. A. Benedek, A. T. Mulder, and C. J. Fennie, J. Solid State Chem. **195**, 11 (2012).
[5]A. T. Mulder, N. A. Benedek, J. M. Rondinelli, and C. J. Fennie, Adv. Funct. Mater. **23**, 4810 (2013).
[6]N. A. Benedek, J. M. Rondinelli, H. Djani, P. Ghosez, and P. Lightfoot, Dalton Trans. **44**, 10543 (2015).
[7]M. J. Pitcher, P. Mandal, M. S. Dyer, J. Alaria, P. Borisov, H. J. Niu, J. B. Claridge, and M. J. Rosseinsky, Science **347**, 420 (2015).
[8]Y. S. Oh, X. Luo, F.-T. Huang, Y.-Z. Wang, and S.-W. Cheong, Nat. Mater. **14**, 407 (2015).
[9]Y. Wang, F.-T. Huang, X. Luo, B. Gao, and S.-W. Cheong, Adv. Mater. **29**, 1601288 (2017).
[10]X. Q. Liu, J. W. Wu, X. X. Shi, H. J. Zhao, H. Y. Zhou, R. H. Qiu, W. Q. Zhang, and X. M. Chen, Appl. Phys. Lett. **106**, 202903 (2015).
[11]M. V. Lobanov, M. Greenblatt, E. N. Caspi, J. D. Jorgensen, D. V. Sheptyakov, B. H. Toby, C. E. Botez, and P. W. Stephens, J. Phys.: Condens. Matter **16**, 5339 (2004).
[12]M. S. Senn, A. Bombardi, C. A. Murray, C. Vecchini, A. Scherillo, X. Luo, and S.-W. Cheong, Phys. Rev. Lett. **114**, 035701 (2015).
[13]A. C. Larson and R. B. Von Dreele, Los Alamos National Laboratory Report No. LAUR, 86, 1994.
[14]W.-K. Zhu, L. Pi, Y.-J. Huang, S. Tan, and Y.-H. Zhang, Appl. Phys. Lett. **101**, 192407 (2012).
[15]See http://rredc.nrel.gov/solar/spectra/am1.5/ for information about the Reference AM 1.5 Spectra.
[16]K. T. Butler, J. M. Frosta, and A. Walsh, Energy Environ. Sci. **8**, 838 (2015).
[17]Y. Zhang, L.-F. Lin, J.-J. Zhang, X. Huang, M. An, and S. Dong, Phys. Rev. Mater. **1**, 034406 (2017).
[18]R. Nechache, C. Harnagea, S. Li, L. Cardenas, W. Huang, J. Chakrabartty, and F. Rosei, Nat. Photonics **9**, 61 (2015).
[19]X. Huang, T. R. Paudel, S. Dong, and E. Y. Tsymbal, Phys. Rev. B **92**, 125201 (2015).
[20]Y. Yuan, T. J. Reece, P. Sharma, S. Poddar, S. Ducharme, A. Gruverman, Y. Yang, and J. Huang, Nat. Mater. **10**, 296 (2011).
[21]P. Kubelka and F. Munk, Z. Tech. Phys. **12**, 593 (1931).
[22]S. F. Matar, V. Eyert, A. Villesuzanne, and M.-H. Whangbo, Phys. Rev. B **76**, 054403 (2007).
[23]G. Kresse and J. Hafner, Phys. Rev. B **47**, 558 (1993).
[24]G. Kresse and J. Furthmüller, Phys. Rev. B **54**, 11169 (1996).
[25]G. Kresse and D. Joubert, Phys. Rev. B **59**, 1758 (1999).
[26]J. P. Perdew, K. Burke, and M. Ernzerhof, Phys. Rev. Lett. **77**, 3865 (1996).
[27]J. P. Perdew, A. Ruzsinszky, G. I. Csonka, O. A. Vydrov, G. E. Scuseria, L. A. Constantin, X. Zhou, and K. Burke, Phys. Rev. Lett. **100**, 136406 (2008).
[28]S. L. Dudarev, G. A. Botton, S. Y. Savrasov, C. J. Humphreys, and A. P. Sutton, Phys. Rev. B **57**, 1505 (1998).